EARTH SURFACE PROCESSES AND LANDFORMS
Earth Surf. Process. Landforms (2015)

Published online in Wiley Online Library
(wileyonlinelibrary.com) DOI: 10.1002/esp.3783

Englacial and subglacial water flow at Skálafellsjökull, Iceland derived from ground penetrating radar, *in situ* Glacsweb probe and borehole water level measurements

Jane K. Hart,[1]* Kathryn C. Rose,[2] Alexander Clayton[1] and Kirk Martinez[2]
[1] Geography and Environment, University of Southampton, Southampton SO17 1BJ, UK
[2] School of Geographical Sciences, University of Bristol, Bristol BS8 1SS, UKElectronics and Computer Science, University of Southampton, Southampton SO17 1BJ, UK

Received 24 July 2014; Revised 24 June 2015; Accepted 30 June 2015

*Correspondence to: J. K. Hart, Geography and Environment, University of Southampton, Southampton, SO17 1BJ, UK. E-mail: jhart@soton.ac.uk

ESPL
Earth Surface Processes and Landforms

ABSTRACT: We reconstruct englacial and subglacial drainage at Skálafellsjökull, Iceland, using ground penetrating radar (GPR) common offset surveys, borehole studies and Glacsweb probe data. We find that englacial water is not stored within the glacier (water content ~0–0.3%). Instead, the glacier is mostly impermeable and meltwater is able to pass quickly through the main body of the glacier via crevasses and moulins. Once at the glacier bed, water is stored within a thin (1 m) layer of debris-rich basal ice (2% water content) and the till. The hydraulic potential mapped across the survey area indicates that when water pressures are high (most of the year), water flows parallel to the margin, and emerges 3 km down glacier at an outlet tongue. GPR data indicates that these flow pathways may have formed a series of braided channels. We show that this glacier has a very low water-storage capacity, but an efficient englacial drainage network for transferring water to the glacier bed and, therefore, it has the potential to respond rapidly to changes in melt-water inputs. © 2015 The Authors. Earth Surface Processes and Landforms published by John Wiley & Sons Ltd.

KEYWORDS: GPR; subglacial hydrology; subglacial processes; debris-rich basal ice; glacier water content

Introduction

The glacial hydrological system modulates ice dynamics and is, therefore, a vital component in understanding how glaciers respond to climate change (Mair *et al.*, 2002; Copland *et al.*, 2003; Clarke, 2005). Glacier motion occurs via mechanisms of ice deformation, sliding and the deformation of subglacial sediments, all of which are influenced by the presence of meltwater. A glacier's hydrological system encompasses water flow and storage through englacial and subglacial environments (Fountain and Walder, 1998; Jansson *et al.*, 2003), both of which may vary spatially and temporally (Iken and Bindschadler, 1986, Mair *et al.*, 2003; Rose *et al.*, 2009).

Studies have shown that the englacial system comprises water within a series of connected and disconnected, centimetre to decimetre sized voids (Pohjola, 1993; Murray *et al.*, 2000), crevasses, or moulins (Nienow *et al.*, 1998; Fountain *et al.*, 2005). The latter two can readily drain water from the glacier surface to its bed (Zwally *et al.*, 2002; Das *et al.*, 2008; Benn *et al.*, 2009). At the ice-bed interface, the subglacial system is composed of connected channelised networks (Röthlisberger (R)-channels (Röthlisberger, 1972) and Nye channels (Nye, 1973)) and less well connected broad and shallow Hooke channels (Hooke *et al.*, 1990), water films, canals (Walder and Fowler, 1994), cavities and 'microcavities' (Kamb, 1991). Water may also flow within subglacial till, where present (Boulton and Jones, 1979). Fountain and Walder (1998) and Gulley *et al.* (2009) argue that water transfer through the glacial hydrological system is characterised as either 'fast' or 'slow' flow. The former occurs via englacial crevasses (Fountain *et al.*, 2005), conduits (Benn *et al.*, 2009; Gulley *et al.*, 2009), and subglacial R-channels (Fountain and Walder, 1998). The latter through connected englacial voids and subglacial linked cavities and Hooke channels (Willis *et al.*, 1990).

Typically, a temperate glacier constitutes four different components: ice, water, debris and air; the relative proportions of these elements may modulate the behaviour of ice. In a glacier, air can be found at the micro-scale within the ice crystal lattice and at the macro-scale as larger centimetre to decimetre sized englacial air pockets. Temperate glaciers are subject to surface melt and surface precipitation, which provide sources of water to the englacial hydrological system. At the bed, water may be generated as a result of pressure melting, frictional melting and englacial inputs.

Typical water contents reported from ground penetrating radar (GPR) surveys of temperate glaciers range from 0–9% (Macheret

and Glazovsky, 2000; Pettersson *et al.*, 2003; Murray *et al.*, 2007). The quantity and distribution of this stored water is important because water content has a strong influence on ice rheology (Duval, 1977), affecting the contribution (rate and amount) of internal ice deformation to net glacier motion. These effects are difficult to predict because water content often varies spatially (Macheret and Glazovsky, 2000; Murray *et al.*, 2000) and temporally (Jacobel and Raymond, 1984; Macheret and Glazovsky, 2000; Irvine-Fynn *et al.*, 2006; Kulessa *et al.*, 2008).

In addition, temperate glaciers typically have a debris-rich basal ice layer (0.1–10 m thick) that is characterised by an elevated water content (Hart and Waller, 1999; Lawson and Elliott, 2003). This occurs as water molecules form a microscopic layer around sediment particles within the ice (Carol, 1947; Hooke *et al.*, 1972). Then water held between the debris/ice layers acts as a lubricant that enhances sliding along these layers (Echelmeyer and Wang, 1987; Cohen, 2000). In turn, the higher water content of the debris-rich layer affects ice rheology and creep rates, whereby creep rates generally increase with water content (Duval, 1977).

Here, we use GPR to calculate the reflectivity of the bed, which together with borehole water-level behaviour and theoretical drainage reconstruction can be used to infer the location and morphology of basal conduits. Our specific objectives were to:

- calculate glacier water content and thereby establish the potential for englacial water storage and ice rheology;
- determine basal reflection strength along GPR transects, in order to map potential subglacial fast flow drainage pathways;
- calculate hydraulic potential for the study site; and
- combine these results with those from subglacial *in situ* monitoring, to present a conceptual hydrological model for Skálafellsjökull.

Field site and Methodology

This study was undertaken at Skálafellsjökull, Iceland, an outlet glacier of the Vatnajökull icecap (Figure 1). The glacier has an area of approximately 100 km^2 and is 25 km in length (Sigurðsson, 1998). The bedrock is Upper Tertiary grey basalts with intercalated sediments consisting of oxidised palaeosols and/or tephra layers (Jóhannesson and Sæmundsson, 1998).

The study site was located on the southern side of the Skálafellsjökull glacier at an elevation of 792 m (a.s.l.) (Figure 1). Here, ice flows south-east towards a local tongue (named Sultartungnajökull), where a large subglacial river emerges from the glacier bed. The study site was divided into two areas, the main study area (hereafter, Site 1) and the smaller eastern study area (hereafter, Site 2).

Data were collected over a series of summer field seasons between 2008 and 2013. GPR surveys were used to map the underlying topography, the internal structure of the ice and to

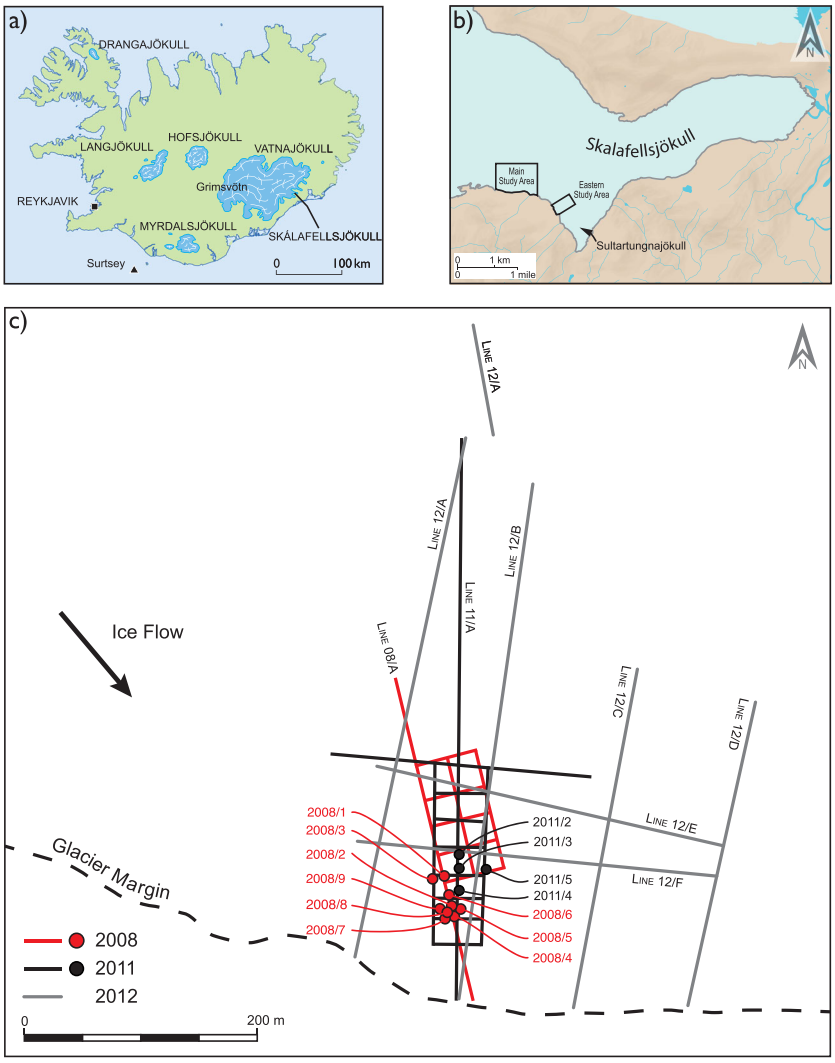

Figure 1. (a) Location of Skálafellsjökull in Iceland. (b) Detail of Skálafellsjökull, showing location of the main study area (Site 1) and the eastern study area (Site 2). (c) Site 1, showing the radar common offset survey grids and boreholes (lines and dots, respectively), from 2008 (red) 2011 (black) and 2012 (grey). This figure is available in colour online at wileyonlinelibrary.com/journal/espl

calculate the composition of ice, air, water and debris within the glacier, as well as calculate the reflectivity of the bed. We use these data, in combination with borehole observations and *in situ* subglacial instrumentation and theoretical drainage reconstructions to reconstruct the glacier's hydrological system.

Sedimentology

Overlying the bedrock is a basalt-rich till, which is composed of numerous large boulders within a very fine matrix (less than 2000 μm) with a mean grain size 53 μm. Grain size was determined through a combination of dry sieving and laser granulometry, and examined with the GRADISTATv5 programme (Blott and Pye, 2001, 2006) and, in particular, using the Folk and Ward method (1957). Small push moraines (<1 m high), are found adjacent to the ice reflecting former glacial marginal positions. Numerous debris bands are evident within the glacier ice and the majority of outcrops are located at the glacier margin. A sample of debris-rich ice was collected close to the margin (in order to determine its debris composition and concentration).

Glacier survey and instrumentation

In 2008 and 2011 survey grids were established on the glacier surface at Site 1 (Figure 1(c)). These grids encompassed an area of ~200 × 50 m and were used as the basis for further investigations (as described below). Site 1 was also resurveyed over a larger area (600 × 300 m) in 2012. In 2013, Site 2 (500 × 50 m) was surveyed (Figure 1(b)). In addition, a long survey line was established in each field season in order to map a larger area of the glacier bed (Line 08/A (2008), Line 11/A (2011), Line 12/A-F (2012)) (Figure 1(c)). Site 2 comprised two lines (50 m apart), oriented perpendicular to the margin, and extending 500 m from the margin.

In order to examine the glacier body and instrument the subglacial environment, boreholes were drilled along GPR transects and within the survey grids with a Kärcher HDS1000DE hot-water drill (Figure 1(c), circles). Videos were filmed in each borehole with a custom made infra-red (900 nm) CCD camera to assess the internal ice structure and glacier bed. Borehole depths were measured with the drill hose and cross-checked against the known camera cable length. In 2008, till was collected from the base of the boreholes with a subglacial sediment sampler attached to a subglacial percussion hammer (Blake *et al.*, 1992). The locations of the survey grids and boreholes were recorded using a differential GPS (dGPS). The three dimensional aspects of the glacier were determined from surface dGPS heights, IS 50 V Landmælinger Íslands data, CNES spot data, measured borehole depths and GPR surveys.

In 2008, the subglacial environment was instrumented using Glacsweb wireless probes (16 cm long, axial ratio 2.9:1) (Hart *et al.*, 2009), set within an environmental sensor network (ESN) (Hart and Martinez, 2006; Martinez and Hart, 2010; Figure 2). The probes were installed, via boreholes, into the underlying till, which was hydraulically excavated (Blake *et al.*, 1992) by maintaining the jet of hot water from the drill at the borehole base for an extended period of time. Once lowered into this space, the till subsequently closed in around the probe (Hart *et al.*, 2006). Probe micro-sensors measured temperature, water pressure, probe deformation, conductivity, and tilt (Table I). Here, only water pressure and temperature results are discussed (specific details of the system are described in Martinez *et al.* (2009). Data were collected every hour and then transferred daily, via radio communications, to a base station located at the glacier surface (Figure 2). The base station was equipped with a weather station and dGPS capabilities. It relayed these and probe data once a day, via GPRS (mobile phone), to a web server at the University of Southampton. The ESN operated from August 2008 to August 2013, inclusive of intermittent periods when the system was disconnected or subject to power failure. When interrupted, weather data were obtained from the nearest national station at Höfn and a transfer function was applied to compute any data gaps. A local dGPS base station (for differential correction) was also mounted on a café situated ~1 km from the study site.

GPR survey

Common offset (CO) surveys were carried out over the survey grids at Sites 1 and 2 (Figure 1), using a *Sensors and Software Pulse Ekko 100* with a 1000 V transmitter system and 50 MHz antennas. A 2 m antenna spacing and 0.5 m sampling interval were used for the CO survey. A custom built sledge was constructed to hold the antennae at the correct distance apart and allow the system to move along the grid transects more readily.

GPR processing

A series of standard processing steps were applied to the CO survey data using the software package ReflexW. Low frequency noise was eliminated (de-wow filter) and a SEC (spreading and exponential compensation) gain was applied to compensate for signal loss with depth. Next a diffraction stack migration and topographic correction were applied. Finally, the ice-bed interface was identified manually in radar echograms from a clear strong reflector. It was then possible to calculate the radar-wave velocity in the whole ice column (v) by comparing the depth of the glacier bed in radar

Table I. Technical specifications for probe micro-sensors

Sensor	Technical specifications	Resolution (step size)	Range
Temperature sensor	DS1631	0.0625°C	–10 - +85°C
Pressure transducer	24PCGFM6G	1.122 kPa	0–1724 kPa
Strain gauges	Strain gauge	1.25 N	0–213 125 N
Conductivity	Resistance bridge	0.005 μS	0–100 μS
Tilt sensors 1 and 2	LIS3LV02DQ	0.000976 g	-/+ 2 g

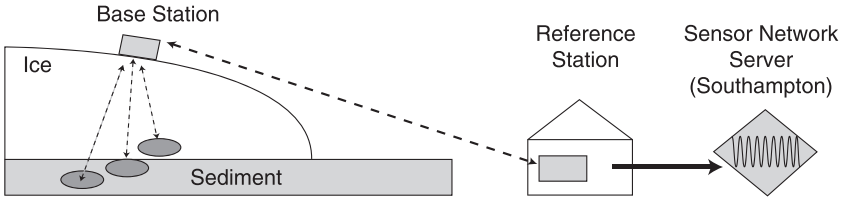

Figure 2. Glacsweb environmental sensor network system.

echograms with measured borehole glacier depths, according to the equation:

$$v = \frac{2h}{t} \tag{1}$$

(see Table II for explanation of all symbols used for this and all subsequent equations).

Subsequently, the GPR data were analysed in order to:

- determine glacier water content by calculating the relative proportions of ice, air, water and debris within the glacier and permittivity changes in the GPR data. These data were then used to calculate the flow parameter in the Nye (1952) creep law;
- map the spatial distribution of subglacial water bodies by calculating the radar basal reflection power;
- produce a map of subglacial hydraulic potential to compare with the distribution of radar basal reflection intensities, in order to determine the most likely locations of subglacial water bodies and the structure of the subglacial drainage system.

Water content

The composition of ice (i), water (*w*), debris (*d*) and air (*a*) within a glacier can be determined according to the permittivity of the glacier body (ε_m). This varies as a function of dielectric permittivities (ε_x) of *x*th components with a volume portion (f_x) (Sihvola *et al.*, 1985), as follows:

$$\varepsilon_m = \sum f_x \varepsilon_x{}^{y} \tag{2}$$

In this case y =1/4 and the permittivity (ε_m) of the mixture is:

$$\varepsilon_m = (c/v)^2 \tag{3}$$

Based on the work of Looyenga (1965), Macheret *et al.* (1993) and Macheret and Glazovsky (2000), permittivity can be rewritten as:

$$\varepsilon_m = \left(\left(P_i \varepsilon_i^{1/4}\right) + \left(P_w \varepsilon_w^{1/4}\right) + \left(P_d \varepsilon_d^{1/4}\right) + \left(P_a \varepsilon_a^{1/4}\right)\right)^4 \tag{4}$$

This demonstrates that total permittivity reflects the sum of the components ice, water, debris and air. Alternatively, the Looyenga (1965) model uses three components (ice, air water) (z =1/3 in Equation (1)) and assumes that the total void space is water filled, in order to estimate water content (w), as follows:

$$w = \left(\varepsilon_m^{\frac{1}{3}} - \varepsilon_i^{\frac{1}{3}}\right) / \left(\varepsilon_w^{\frac{1}{3}} - \varepsilon_i^{\frac{1}{3}}\right) \tag{5}$$

Although Endres *et al.* (2009) have argued that this model slightly underestimates water content, this is the most commonly used mixing model and so is useful for comparison with other studies (Macheret *et al.*, 1993; Murray *et al.*, 2000; Hausmann and Behm, 2011). We can, therefore, use this method to determine at least a minimum value for water content within the main body of the glacier.

It is also possible to calculate the radar velocity through the debris-rich ice by knowing the composition of the debris and its concentration (assuming a two component model of ice and debris, Lichtenecker (1926), after Zakri *et al.*, 1998):

$$\varepsilon_m = \exp(P_i \ln \varepsilon_i + P_d \ln \varepsilon_d) \tag{6}$$

The air within the glacier will be stored either as small bubbles within the ice and/or as larger scale features such as cavities or crevasses. Bradford *et al.* (2009) have calculated how the bubble content of ice decreases with depth, as follows:

$$P_{a(k+1)} = \frac{KT_0}{\left[g p_i \Delta z \sum_{k=1}^{n} \left(1 - P_{a(k)}\right] + P_0\right.} - K\beta' \tag{7}$$

Then they use a three-component CRIN (complex refractive index method) equation (Wharton *et al.*, 1980) to calculate water content with depth:

$$P_w = \frac{\sqrt{\varepsilon_m} - \sqrt{\varepsilon_i} - P_a\left(\sqrt{\varepsilon_a} - \sqrt{\varepsilon_i}\right)}{\sqrt{\varepsilon_w} - \sqrt{\varepsilon_i}} \tag{8}$$

Using Equation (6), we use the GPR data to calculate the distribution of air content within the glacier, and use this value in Equation (7) to calculate a depth averaged maximum water content.

It is then possible to determine the effect of water content on the flow parameter in the creep law (A) (Duval, 1977), as follows:

$$\mathrm{A} = (3.2 + 5.8\mathrm{w}) \times 10^{-15} (\mathrm{kPa})^{-3} \mathrm{s}^{-1} \tag{9}$$

This could be used in the shallow approximation model (Nye, 1952; Paterson, 1994), (which ignores longitudinal and transverse stresses) to estimate the proportion of ice flow solely from internal deformation (U_c):

$$u_c = \frac{2A}{n+1} (p_i g \sin\alpha)^n h^{n+1} \tag{10}$$

Basal reflection

Numerous researchers (Winebrenner *et al.*, 2003; MacGregor *et al.*, 2007; Matsuoka *et al.*, 2010; Jacobel *et al.*, 2009, 2010) have shown that the power of electromagnetic energy returned from the subglacial interface is determined by three factors: the dielectric properties of the reflector (the basal reflectivity) (*R*), losses due to geometric spreading (which are related to glacier depth), and losses due to dielectric attenuation within the ice (L_a). These factors are represented as:

$$P_r = P_t \frac{a_t}{4\pi} \frac{1}{(2h)^2} R \exp\left(-\frac{2h}{L_a}\right) \tag{11}$$

Most researchers take the $\log_{10}$ of both sides of Equation (11) and calculate one-way attenuation rate N_a, which is related to L_a by:

$$N_a = \frac{10^3 (10 log_{10} e)}{L_a} \tag{12}$$

Dielectric attenuation, which is primarily a function of ice temperature and impurity content, can be calculated using three methods:

(i) $$N_a \approx 0.912\sigma \tag{13}$$

where

$$\sigma = \sigma_0 \exp\left[\frac{E_0}{B}\left(\frac{1}{T_r} - \frac{1}{T}\right)\right] \tag{14}$$

Table II. Explanation of symbols and values used

Symbol	*Parameter*	*Value of Constants*	*Units*	*Equation Number*
v	Radar-wave velocity in the whole ice column		m ns^{-1}	1,3
h	One-way path length (ice thickness)		m	1,9,10,15
t	Two-way radar traveltime		ns	1
ε_m	Permittivity of the whole mixture		F m^{-1}	2,3,4,5,7
ε_x	Permittivity of different components (x),. ice, water, debris or air).		F m^{-1}	2
y	Number of components			2
f_x	Volume portion of each component		1/x	2
c	Velocity of light	3×10^8	m s^{-1}	3
P	Relative percentage			4,5,6,8
ε_I	Permittivity of ice	3.19	F m^{-1}	4,5,6,8
ε_W	Permittivity of water	86	F m^{-1}	4,6,8
ε_D	Permittivity of debris	8.5	F m^{-1}	4,6
ε_A	Permittivity of air	1	F m^{-1}	4,8
K	Gas constant	8.314	J K^{-1} mol^{-1}	8
T_0	Triple point temperature of water	273.15	K	8
Δz	Depth step	1	m	8
β'	Rate of change of the melting point with pressure for air-saturated water (Paterson, 1994)	0.000098	K Pa^{-1}	8
P_0	Atmospheric pressure	101.325	K Pa	8
U_c	Creep velocity		m a^{-1}	10
A	Flow parameter		a^{-1} bar^{-3}	9,10
n	Glen's law constant	3		10
α	Glacier slope angle	3	degrees	10
p_i	Density of ice	917	kg m^{-3}	10
g	Acceleration due to gravity	9.81	m s^{-2}	10
w	Water content		%	6, 10
P_t	Transmitted power		dB km^{-1}	11
P_r	Returned power		dB km^{-1}	11,16
P_{ro}	Mean reflected power		dB km^{-1}	11,16
a_t	Antenna gain function		dB	11
h_o	Mean one-way ice thickness from all the bed reflections		m	16
R	Reflectivity of the target interface (an internal layer or the bed)		dB	11
L_a	Mean attenuation length due to dielectric loss		m	11
N_a	One-way attenuation rate		dB km^{-1}	12,13,15
σ	Conductivity of ice under investigation		W mK^{-1}	13,14,15
σ_0	Conductivity of pure ice	9.2	μS m^{-1}	14
E_0	Activation energy of pure ice	0.55	eV	14,15
B	Boltzmanns constant	8.617×10^{-5}	eV k^{-1}	14
T_r	Reference temperature	251	K	14
T	Measured temperature		K	14
p_w	Density of water	1000	kg m^{-3}	17
s	Ice surface elevation		m	17
z	Ice base elevation		m	17
k	Spatially uniform flotation fraction P_w/P_i			17
P_w	Water pressure		K Pa	17
P_i	Ice overburden pressure		K Pa	17

(ii)
$$N_a = \frac{10^3(10\log_{10}e)\sigma}{cE_0\sqrt{\varepsilon_i}} \tag{15}$$

iii. where the reflection is not constant along the transect (MacGregor *et al.*, 2007) a graphical method can be used (all values of relative bed echo returned power (corrected for inverse square losses) are plotted against depth). Power (P_r) values are obtained by summing the squared amplitude under the bed echo wavelet (Gades *et al.*, 2000):

$$\frac{P_r}{P_{ro}} = \frac{h_0^2}{h^2}\exp\left[-\frac{2}{L_a}(h-h_0\right] \tag{16}$$

L_a is found from a nonlinear least-squares fit and then is converted to a depth-averaged attenuation rate using Equation (12).

We take the mean attenuation value from these three methods, and apply this as the best-fit line to the data (returned power vs depth). The distance from the fitted line is a measure of relative basal reflectivity (R) for each point (Jacobel *et al.*, 2009, 2010).

Hydraulic potential

The glacier depths determined within both study sites were used to make a realistic estimate of glacier depths in the surrounding area. With this information a map of subglacial hydraulic potential (Φ) was created using the method outlined by Willis *et al.* (2012), adapted from Shreve (1972) and Rippin *et al.* (2003), as follows:

$$\Phi = kp_i g(s-z) + p_w gz \tag{17}$$

where k is the ratio of water pressure to ice overburden (P_w/P_i). When k = 0, water pressure is at atmospheric pressure and

when $k = 1$, water pressure equals ice overburden pressure ($P_w = P_i$). We calculated eleven steady-state subglacial water conditions from $k = 0$ to $k = 1$ at increments of 0.1 k, over sixty 250 m × 250 m grid squares, across the southern part of the glacier. The map of hydraulic potential produced was then compared with the distribution of radar basal reflection power (see below) to determine the most likely locations of subglacial water bodies.

Results and Discussion

Glacier survey and instrumentation

A series of englacial debris bands, approximately 1 m thick, were identified at the glacier surface. Bands typically comprised 4 to 10 thin clast layers, approximately 1–2 cm thick. The majority of clasts measured less than 1 cm in length (a-axis). In places, the debris included angular reddish-brown clay-rich clasts sourced from outcrops of reddish-brown clays (derived from Tertiary oxidised palaeosols and/or tephra layers) common to the local area. Given the location, geometry and concentration of the debris bands we estimate the glacier body (within the main study area) had a debris concentration of approximately 0.5%.

Towards the margin the number and density of these debris bands increased as debris-rich ice at or close to the base of the glacier became exposed at the glacier margin. The depth of this layer varied along the margin, from approximately 0.5–2.0 m (taking the angle of the outcrop into account). The sediment concentration within this debris-rich ice was 13% by weight.

Borehole depths ranged between 57 m and 86 m (Table III). Most boreholes remained water filled each year both during and after drilling. Video images of these water filled boreholes showed a very similar pattern of homogeneous ice with either debris and till at the base (however images from the ice base were poor, due to fine sediments from the till). There were very few fractures, voids or conduits visible in the ice.

In contrast, the images from those boreholes that drained during drilling were clearer and more varied. In borehole 2008/2, approximately 1 m above the base, the drill entered an ice-floored cavity (size greater than the field of view of the camera), where the borehole drained. The drill then passed through a further approximately 0.3 m of debris-rich ice before then reaching till. We interpret this cavity as a pre-existing feature, probably an englacial conduit, close to where it meets the subglacial system.

In borehole 2008/5, the drill entered a cavity (approximately 1.5 m deep, area greater than the field of view of the camera) where the borehole drained. This cavity had a till base (with boulders) and debris-rich ice on the sides. Blocks of debris-rich ice, which must have been detached from the cavity roof or walls, were also visible. We interpreted this feature as a basal cavity. In borehole 2011/4, video footage recorded fast moving water in one direction. The velocity of the water was estimated to be >0.1 m s^{-1} from the video footage by tracing the movement of particles across the different frames. From this we inferred the presence of a drainage pathway.

Till samples were extracted from five boreholes in 2008 from a range of depths and locations (Table III). These findings, in combination with the video evidence for till at the base of all the boreholes (apart from 2011/4 where a drainage pathway was observed), suggest that till covered the majority of the glacier bed in the study area.

Six probes were deployed at the base of boreholes in 2008 (Table III), and four returned data for longer than 3 days (see Table IV for average results). Subglacial temperatures varied around 0°C (average of –0.034°C). Water pressures (in metres water equivalent, m w.e.) were generally high between 2008 and 2010 (mean $k = 0.75$) (Figure 3). Values were particularly high during the summer of 2010 (mean $k = 0.8$), with high fluctuations during the spring of 2009 ($k = 1.1$–0.1, mean $k = 0.74$),

Table III. Borehole details

Borehole number	*Depth (m)*	*Behaviour*	*Probe (2008)*	*Till sample collected (2008)*	*Mean radar velocity (m ns^{-1})*
2008/1	73.0	Borehole remained filled with water	*26*	✓	0.183
2008/2	61.0	Borehole drained at 60 m down during drilling Cavity feature observed with a till at base			0.176
2008/3	69.0	Borehole remained filled with water		✓	0.179
2008/4	58.0	Borehole remained filled with water	*21*		0.178
2008/5	61.5	Borehole drained at 60 m down during drilling Cavity observed with till base			0.179
2008/6	65.5	Borehole drained after 30 min after drilling finished	27	✓	0.178
2008/7	57.0	Borehole remained filled with water	*24*		0.177
2008/8	58.0	Borehole remained filled with water	23	✓	0.170
2008/9	59.5	Borehole remained filled with water	*25*	✓	0.178
2008 mean	**62.5**				**0.177 (s.d.0.003)**
2011/2	72.5	Borehole remained filled with water			0.172
2011/3	70.2	Borehole remained filled with water			0.180
2011/4	62.0	Borehole drained at 60 m down during drilling Fast flowing water at base			0.173
2011/5	74.5	Borehole remained filled with water			0.174
2011 mean	**69.8**				**0.174 (s.d.0.003)**
2012/4	86.0	Borehole remained filled with water			0.174
2012/5	69.0	Borehole remained filled with water			0.182
2012/6	67.5	Borehole remained filled with water			0.189
2012/7	68.8	Borehole remained filled with water			-
2012/8	67.0	Borehole remained filled with water			-
2012/12	26.0	Borehole remained filled with water			0.170
2012 mean	**64.0**				**0.179 (s.d.0.008)**
All	**64.1**				**0.177 (s.d. 0.005)**

Table IV. Glacsweb probe data

Probe	*Mean temperature (s.d.)*	*Mean k (water pressure/ice overburden pressure) (s.d.)*			
		Summer 2008	*Spring 2009*	*Winter–spring 2009/10*	*Summer 2010*
21	+0.003°C (0.004)	0.97 (0.02)	0.94 (0.01)	0.79 (0.05)	-
24	–0.119°C (0.02)	0.95 (0.01)	0.77 (0.36)	-	-
25	+0.006°C (0.01)	0.59 (0.23)	0.62 (0.02)	0.52 (0.02)	0.5 (0.18)
26	–0.048°C (0.03)	0.97 (0.05)	0.62 (0.07)	-	-
Mean	–0.034°C (0.058)	0.87 (0.07)	0.74 (0.03)	0.66 (0.04)	0.5 (0.18)

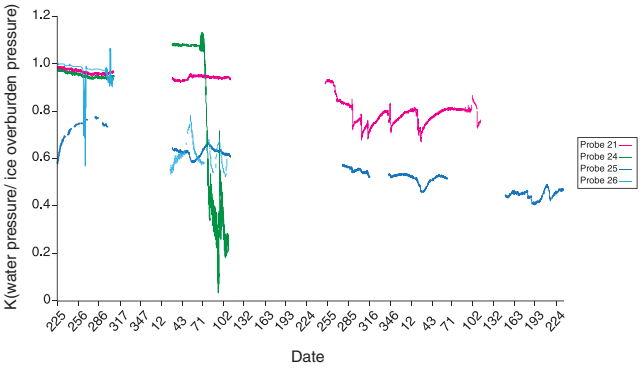

Figure 3. Glacsweb probe results (k = water pressure/ice overburden pressure) for two years, August 2008 to August 2010. This figure is available in colour online at wileyonlinelibrary.com/journal/espl

and then smaller fluctuations during the autumn, winter and spring of 2009/10 (mean k = 0.66).

The surface velocity of the glacier at the Base Station was relatively low (average over the 3 years was 3.78 m a^{-1} +/- 0.58; ice depth 54 m). Ice flow was from north-west to south-east, and the slope angle in this direction was approximately 3°. Ablation in the study area was measured as approximately 0.05 m d^{-1} during the summers of 2008 and 2011.

GPR

Radar-wave velocity of ice

Figure 4 shows radar echograms along Lines 08/A and 11/A (Figure 1(c)), where a strong reflection signal clearly showed the bed of the glacier. The radar-wave velocities for 2008, 2011 and 2012 were very similar (Table III). The overall mean for the three years was 0.177 m ns^{-1}, with an error of 2.75% (s.d. as a percentage of the mean). This is the same as the error discussed in detail by Barrett *et al.* (2007). The small standard deviation implies that the boreholes were relatively straight and thus, represented the true ice thickness. This mean value was used to calculate the depth of the glacier in 2013.

Evidence from the boreholes and the glacier margin indicated the presence of a thin (but variable) layer of debris-rich ice at the glacier base. We have used an average value of 1 m for subsequent calculations. The debris is mostly composed of basalt, whose constituents are pyroxene, which has a dielectric constant of 8.5 (Olhoeft, 1989; Martinez and Byrnes, 2001).

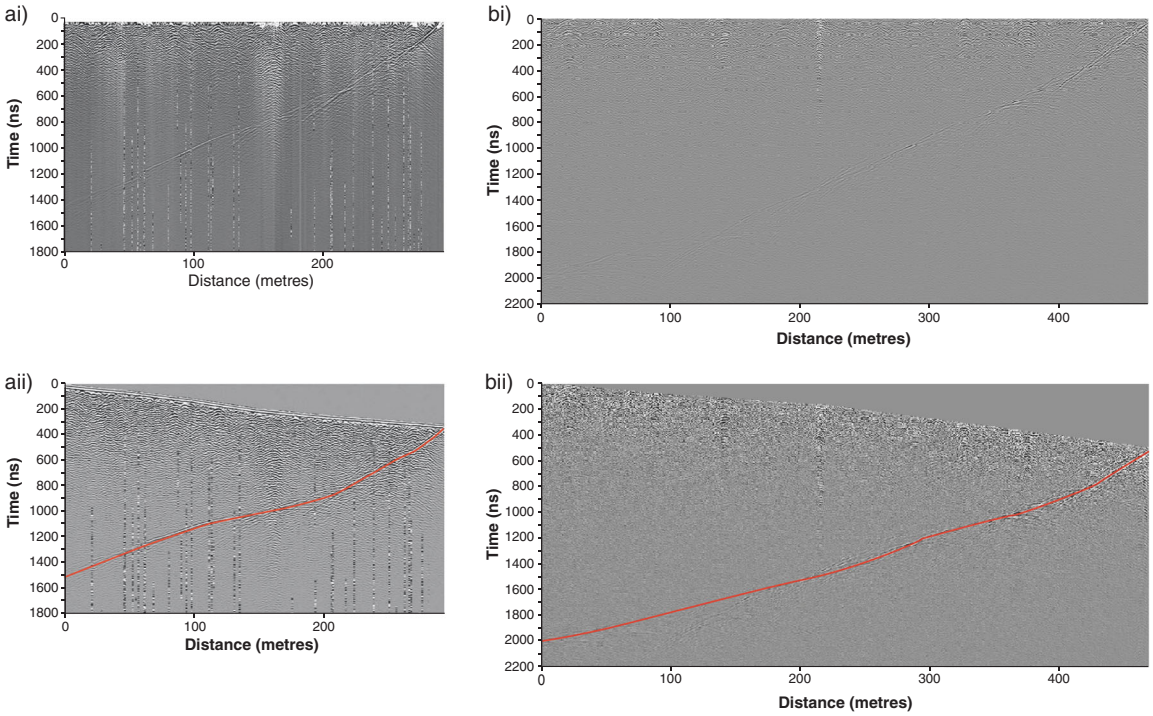

Figure 4. Radar echograms (ice flow into the page): (ai) Line 08/A -unprocessed data; (aii) Line 08/A with topographic correction and differential stack migration, with the glacier bed marked by the red line; (bi) Line 11/A- unprocessed data; (bii) Line 11/A with topographic correction and differential stack migration, with the glacier bed marked by the red line. This figure is available in colour online at wileyonlinelibrary.com/journal/espl

Given that debris-rich ice has a debris concentration of 13%, the calculated radar-wave velocity (using Equation (5)) is 0.158 m ns^{-1}. This is similar to values derived for debris-rich ice (0.153 m ns^{-1}) (Arcone *et al.*, 1995) and massive silty ice in permafrost (0.156 m ns^{-1}) (Arcone and Delaney, 1989).

Water content of glacier layers

The glacier is composed of two layers, the main body and a thin (1.0 m) debris-rich ice layer. Although there is a wide range of measured radar-wave velocities within glaciers, the normal value for temperate ice is 0.168 m ns^{-1} (Davis and Annan, 1989; Macheret and Glazovsky, 2000). Values lower than this suggest high glacier water contents (Macheret *et al.*, 1993) and/or the presence of debris (Arcone *et al.*, 1995). Higher values indicate very low/zero water contents and the presence of air pockets, such as crevasses, drained conduits, cavities and air bubbles (Moorman and Michel, 1998; Bradford *et al.*, 2009).

We can calculate the relative proportions of air, ice and water (Equation (4)) in the two zones (Table V). In the lower debris-rich layer, we apply the technique of Macheret and Glazovsky (2000), and use the calculated permittivity (ε_m) of the mixture, the known debris content and assume that all the voids are filled with water. This suggests a maximum water content of 2%.

In the main part of the glacier, we use the Looyenga (1965) model to calculate minimum water content, which is zero (since the radar-wave velocity is greater than 0.168 m ns^{-1}). Using Equation (4), we can use the measured mean radar-wave velocity to estimate glacier air volume as 10.5% (+3.5/-2.0%).

Trapped air bubbles may occupy 15–20% ice volume in the upper layers of a glacier (West *et al.*, 2007; Bradford *et al.*, 2009), but there is a significant decrease in bubble content with depth (Bradford *et al.*, 2009). Bradford *et al.* (2009) showed that air content may decrease from 10% at the surface to <5% at 10 m below the surface. We use our calculated air content value of 10.5% at the surface, to calculate the average bubble content over the whole glacier thickness (Equation (6)). From this, we can estimate that 35% of air was stored within air bubbles and 65% in larger-scale cavities and moulins (macroporosity).

It is very likely that temperate ice contains a small amount of water at the ice grain boundaries (reported up to 1.4% in the laboratory; Raymond and Harrison, 1975). We then calculate maximum water content by using the largest uncertainty values of measured ice radar velocity and calculated air content in Equation (7), but inserting a combined ice and debris value calculated from Equation (5) into the 'ice' values (Table V). This gives a maximum water content of 0.03%.

Effect of water content on the flow parameter in the creep law

The water content results (Table V) are used to calculate the effect of water/debris content on glacier velocity. The flow parameter determined for the main body of the glacier (A = 0.1 yr^{-1} bar^{-3}) was much lower than that in the debris-rich basal ice (A = 0.47 yr^{-1} bar^{-3}). However, the combined effect of the two layers gave a flow parameter of A = 0.20 yr^{-1} bar^{-3}, which is very similar to the rate determined by Paterson (1994) for temperate ice (A = 0.21 yr^{-1} bar^{-3}).

Basal reflectivity

Table VI details radar-wave attenuation calculated by the three methods discussed above. The results show an average of 62.16 dB km^{-1}, with an error of 3.8% (s.d. as a percentage of the mean). The mean value for pure ice is 56.23 dB km^{-1} (error of 3.6%). Both the glacier's debris and high air content affect the attenuation rate. The values of basal reflection (R) are shown in Figure 5. Following Jacobel *et al.* (2010), these values are then plotted as a histogram and three peaks are identified (Figure 6). The lowest peak (< –3 dB) reflects dry till or bedrock, the main central peak (–3 to 10 dB) indicates wet till, and the high peak (>10 dB) represents a water body.

We calculate the relative percentage of each bed type over the area surveyed both in 2008 and 2011 (Table VII). The location of high values of R along the GPR transects are shown in Figure 7(a) (red and black boxes). These areas are interpreted as water bodies, which vary in width along the transect from 0.5–15 m (average of 3 m). This is validated by borehole video footage, which showed evidence of subglacial water flow at Borehole 2011/4 (Table III; Figs. 1(c) and 7(a)). These water bodies were found in a similar location in both years. Figure 7 (b) displays two interpretations of subglacial water distribution across the 2008 and 2011 survey grids. The water bodies identified flow north-west to south-east and could either reflect a series of relatively straight R-channels (with ~27 m of separation),

Table VI. Values for attenuation rate

	Attenuation rate dB km^{-1}	
Method	**Skálafellsjökull**	**Pure ice**
(i) Equation (13)	64.89	54.80
(ii) Equation (15)	60.76	57.67
(iii) Equation (16)	63.83	-
Mean	63.16 (s.d. 2.14)	56.23 (s.d. 2.03)

Table V. Glacier stratification (with errors as discussed in the text)

			Percentage non-ice components (%)			
				Water		
Glacier stratification	**Thickness (m)**	**Ice radar velocity (m ns^{-1})**	**Air**	**Min.**	**Max.**	**Debris**
Main layer	63.1[i]	0.177[i] +/- 0.003	10.5[v] +/-5.5 (3.7 air bubbles, 9.1 crevasses and moulins[vii])	0[iii]	0.3[vii]	0.5[i]
Basal layer	1[i]	0.158[ii] +/- 0.003	0[iv]	2[vi] +0.7/-0.8		13[i]

i = measured, ii = calculated from Equation (6), iii = calculated from Equation (5), iv = assuming all voids are filled with water, v = calculated from Equation (4) (using iii), vi = calculated from Equation (4) (using iv), vii = calculated from Equation (7), viii = calculated from Equations (6) and (8).

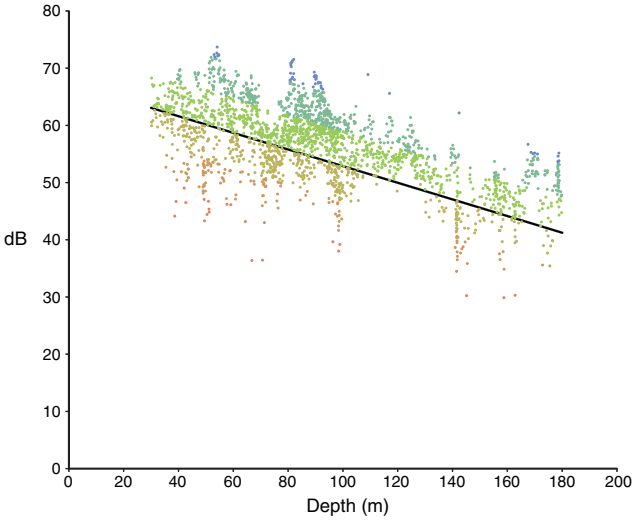

Figure 5. Plot of basal reflected power (corrected for inverse square losses) against ice depth. The line represents a least-squared line with the slope of the mean dielectric attenuation. The value of power above or below the fitted line is a measure of the relative basal reflectivity (*R*). This figure is available in colour online at wileyonlinelibrary.com/journal/espl

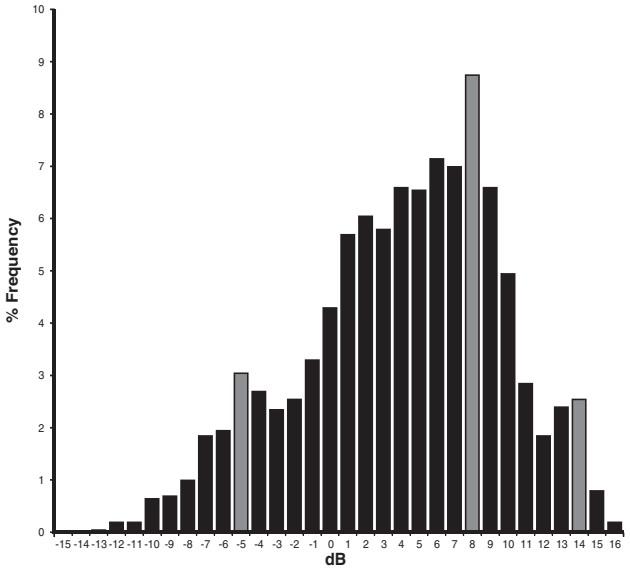

Figure 6. Histogram of the relative basal reflectivity (*R*).

Table VII. Percentage cover of the different bed types (see text for details)

Year	High *R*	Middle *R*	Low *R*
2008	6.5%	83%	10.5%
2011	6.0%	84%	10.0%

or more likely a series of interconnected 'braided' channels (Hock and Hooke, 1993). There may also be disconnected elements, such as cavities, in regions where flowing water was not observed, but is inferred from high *R* values.

Subglacial hydraulic potential

The results of the theoretical hydraulic potential analysis are shown in Figure 8. At high values of *k* (>0.5), there

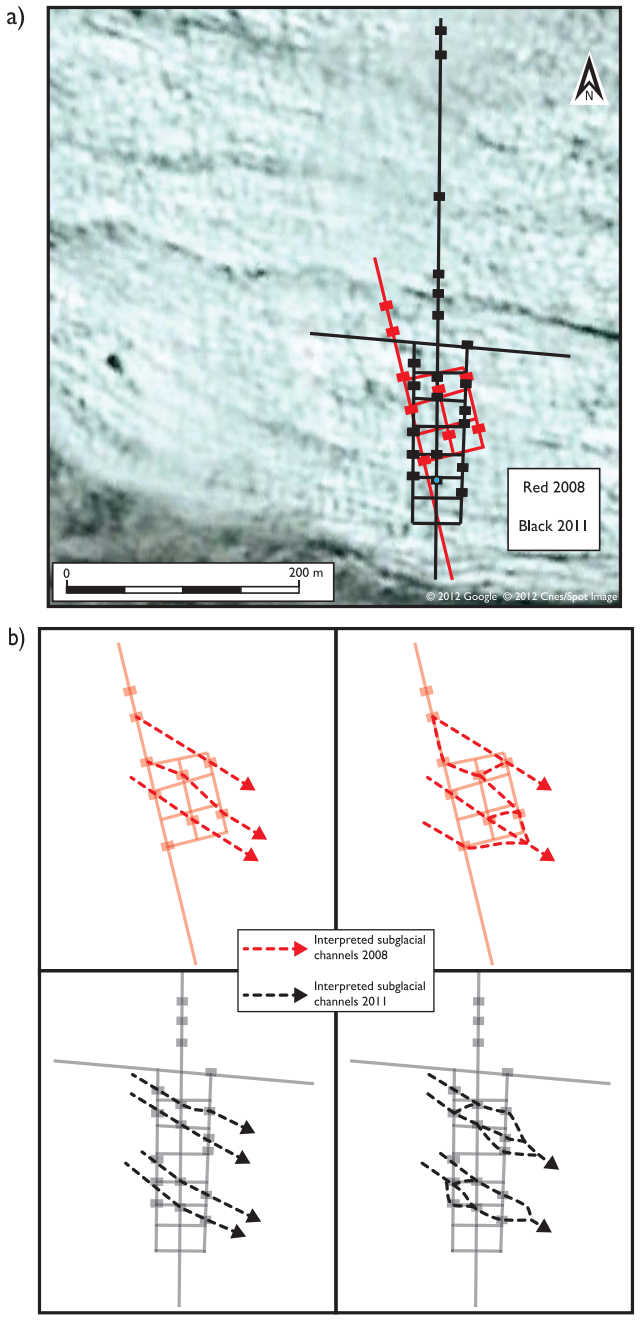

Figure 7. (a) Location of water bodies along the GPR transects, determined from relative basal reflectivity (black and red boxes) and borehole video footage (blue dot); (b) inferred location and structure of subglacial channel pathways across the main survey grid areas. This figure is available in colour online at wileyonlinelibrary.com/journal/espl

is a very high hydraulic potential gradient across the glacier bed from north-west to south-east. At intermediate values of *k* (0.3–0.5) there is a weaker hydraulic potential gradient from north-west to south-east. At low values of *k* (<0.3) the gradient is dominantly oriented north-east (downslope).

In comparison, the values of *k* derived from probe water pressures, in both summer (*k*=0.76) and winter (*k*=0.66), indicate that water would flow from west to east (see also Figure 3, Table IV). This was also shown by the GPR results. It is only during short periods in the winter 2009/2010 that the probe *k* values drop below 0.3 and water flow may be diverted towards the glacier centre.

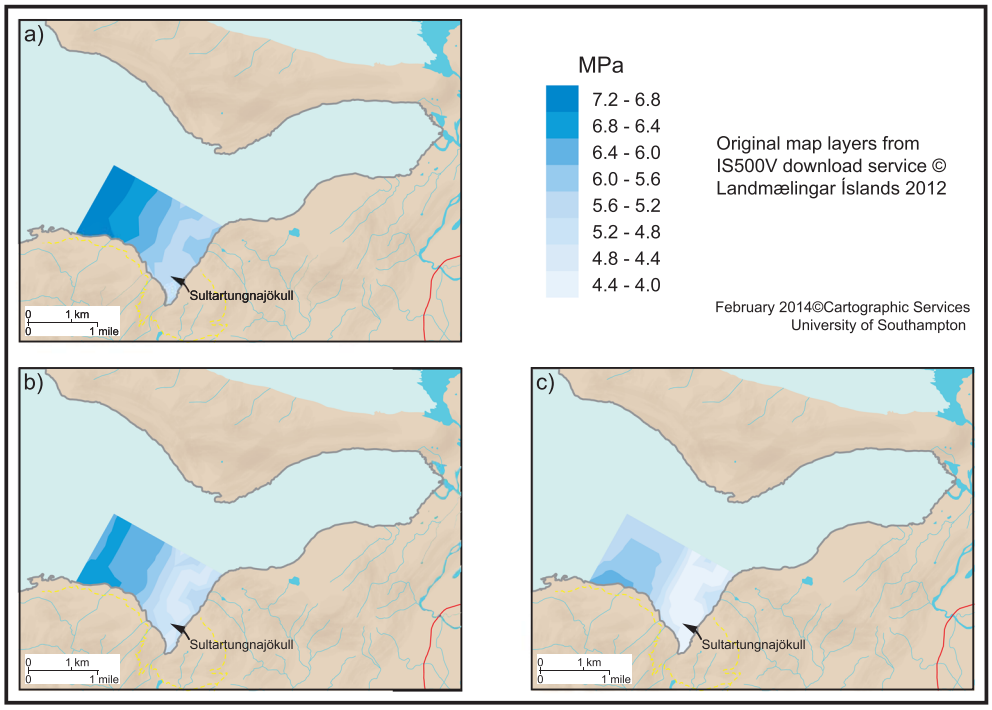

Figure 8. Hydraulic potential contours (in MPa), where: (a) k=0.8; (b) k=0.3, and (c) k=0. This figure is available in colour online at wileyonlinelibrary.com/journal/espl

Hydrological Model

We now bring these analyses together to discuss englacial water flow, the effect of subglacial debris on ice rheology, and the location and form of subglacial drainage pathways.

Englacial water flow

The GPR survey of Skálafellsjökull showed that the glacier comprised two distinct layers: the main body of the glacier with 0–0.3% water content and 10.5% air content; and a lower debris-rich basal ice layer, with a 2% water content. The data also showed two contrasting patterns. First, the main body of the glacier had a low water content and a high macro-porosity, where 65% of air content was associated with crevasses and moulins. These characteristics have rarely been described from temperate glaciers. Second, on drilling the boreholes, most borehole water did not drain, either englacially or subglacially, which implies that the drainage system was poorly connected. Traditionally, low drainage connectivity might imply a high degree of water storage due to a reduction in water transfer capabilities. However, the low water content determined for the glacier suggests that water was unable to 'leak' into englacial voids due to poor network connectivity. Video evidence also showed that the glacier had few visible englacial voids, fractures or conduits. Thus, we infer that the glacier was not substantially permeable, and that any water was concentrated in major drainage pathways, such as crevasses and moulins, that linked directly to the bed.

The high macro-porosity of the main glacier body facilitates a the development of a 'fast' englacial drainage system, allowing surface water to pass very efficiently through the glacier and reach the bed (Catania *et al.*, 2008; Das *et al.*, 2008; Hart *et al.*, 2011b; Sugiyama *et al.*, 2011). Such conditions are commonly associated with enhanced glacier sliding (Iken *et al.*, 1993; Zwally *et al.*, 2002), since there is a localised rapid transit rate and little or no englacial storage.

Once the surface melt reaches the debris-rich ice, the higher water content of this layer suggests that englacial water can be stored there. The storage may comprise connected microscopic water layers around particles within the ice (Carol, 1947; Hooke *et al.*, 1972). Given a mean summer ablation rate of 0.05 m w.e. d^{-1}, over a 1 m^2 area, the debris-rich basal ice could potentially store 0.02 m w.e. d^{-1}, supplying 0.03 m w.e. d^{-1} to the till and/or subglacial drainage system. This layer would have filled during the early part of the summer. It may then provide both slow flow, as water moves through the layer, and fast flow, via the downward extension of crevasses and moulins from the ice above (Fountain *et al.*, 2005; Gulley *et al.*, 2009).

Subglacial water flow

Theoretically, the subglacial hydrological system comprises both drainage through the till and at the ice–till interface. The high water pressures recorded by the probes, combined with high basal reflectivities in GPR data showed that 85% of the bed constituted saturated till. In comparison, a study at Briksdalsbreen, Norway, showed that only 55% of the glacier bed was underlain by saturated till (Hart *et al.*, 2011a). The high percentage of saturated till recorded at Skálafellsjökull indicates a high till water storage capacity. Slow water flow (Darcian flow) will exist in the till and unconnected water bodies may also form (Fountain and Walder, 1998).

Borehole video footage and drainage events demonstrated that only a few boreholes intersected with a connected subglacial drainage system. The reflectivity study showed that approximately 6% of the study area each year was underlain by water bodies (Table VII). The bed appears to have a high number of small high reflective areas, whose spatial arrangement fits best as a series of braided channels, aligned parallel with the ice flow direction and with a gradient of 2.6° (s.d. 0.8). The hydraulic potential modelling showed this direction of flow was maintained throughout the year, with the exception of spring when water could flow north, towards the centre-line of the glacier.

We have shown that at Skálafellsjökull, surface melt water passes via crevasses and moulins to the bed, rather than through a slow connected englacial void system. Water is stored in the debris-rich basal ice layer, till, and at the ice–bed interface. The latter is a combination of disconnected water bodies and subglacial braided channels that flow perpendicular with the glacier margin (in the direction of ice flow), and emerge at Sultartungnajökull, the south-eastern tongue of the glacier, where there is a major outlet river (Figure 1(b)).

Conclusion

Using GPR, field observations and instrumentation, this study has determined the internal structure of the glacier, and we present a hydrological model of Skálafellsjökull. The main glacier body has a very low water content (with high macro-porosity) and the base consists of a thin debris-rich basal ice layer with a 2% water content. The glacier itself is underlain by till.

Since the glacier has a very low water content and high macro-porosity, meltwater reaches the bed almost entirely by fast flow, via crevasses and moulins. Once the water is at the bed it is stored within the debris-rich basal ice layer, as well as in the till and/or in disconnected bodies at the ice–bed interface. These elements also facilitate slow subglacial flow. In addition, there may be braided channels at the ice–bed interface which are oriented with ice flow direction, but parallel with the ice margin. These follow hydraulic potential gradients when water pressures were high during much of the year. A glacier of this nature has little storage capacity, and so has the potential to respond rapidly to changes in melt-water inputs.

Acknowledgements—The authors would like to thank the Glacsweb Iceland 2008, 2011, 2012 team (and Andrew Turner and Tom Bishop in 2013) for help with data collection, and thanks to Dr Laura Edwards for dGPS processing and Sam Buckley for help with GPR processing. Thanks also go the Mark Dover in the Cartographic Unit for figure preparation. We also wish to thank two anonymous referees for their very helpful comments. This research was funded by the ESPRC and the Leverhulme Trust and the GPR was loaned from the NERC Geophysical Equipment Facility.

References

Arcone SA, Delaney AJ. 1989. Investigations of dielectric properties of some frozen materials using cross borehole radiowave pulse transmissions. *CRREL* Report 89.

Arcone SA, Lawson DE, Delaney AJ. 1995. Short-pulse radar wavelet recovery and resolution of dielectric constants within englacial and basal ice of Matanuska Glacier, Alaska, USA. *Journal of Glaciology* **41**: 68–88.

Barrett BE, Murray T, Clark R. 2007. Errors in radar CMP velocity estimates due to survey geometry, and their implication for ice water content estimation. *Journal of Environmental and Engineering Geophysics* **12**: 101–111.

Benn D, Gulley J, Luckman A, Adamek A, Glowacki PS. 2009. Englacial drainage systems formed by hydrologically driven crevasse propagation. *Journal of Glaciology* **55**(191): 513–523.

Blake EW, Clarke GKC, Gerrin MC. 1992. Tools for examining subglacial bed deformation. *Journal of Glaciology* **38**: 388–396.

Blott SJ, Pye K. 2001. GRADISTAT: a grain size distribution and statistics package for the analysis of unconsolidated sediments. *Earth Surface Processes and Landforms* **26**: 1237–1248.

Blott SJ, Pye K. 2006. Particle size distribution analysis of sand-sized particles by laser diffraction: an experimental investigation of instrument sensitivity and the effects of particle shape. *Sedimentology* **53**(3): 671–685.

Boulton GS, Jones AS. 1979. Stability of temperate ice caps and ice sheets resting on beds of deformable sediment. *Journal of Glaciology* **24**: 29–44.

Bradford JH, Nichols J, Mikesel TD, Harper JT. 2009. Continuous profiles of electromagnetic wave velocity and water content in glaciers: an example from Bench Glacier, Alaska, USA. *Annals of Glaciology* **50**(51): 1–9.

Carol H. 1947. The formation of *roches moutonnées*. *Journal of Glaciology* **1**(2): 57–59.

Catania GA, Neumann TA, Price SF. 2008. Characterizing englacial drainage in the ablation zone of the Greenland ice sheet. *Journal of Glaciology* **54**(187): 567–578.

Clarke GKC. 2005. Subglacial processes. *Annual Review of Earth and Planetary Sciences* **33**: 247–276.

Cohen D. 2000. Rheology of ice at the bed of Engabreen, Norway. *Journal of Glaciology* **46**(155): 611–621.

Copland L, Sharp MJ, Nienow PW. 2003. Links between short-term velocity variations and the subglacial hydrology of a predominantly cold polythermal glacier. *Journal of Glaciology* **49**(166): 337–348.

Das SB, Joughin I, Behn MD, Howat IM, King MA, Lizarralde D, Bhatia MP. 2008. Fracture propagation to the base of the Greenland Ice Sheet during Supraglacial Lake Drainage. *Science* **320**(5877): 778–781.

Davis JL, Annan AP. 1989. Ground penetrating radar for high resolution mapping of soil and rock stratigraphy. *Geophysical Prospecting* **37**: 531–551.

Duval P. 1977. The role of water content on the creep rate of polycrystalline ice. *IAHS* **118**: 29–33.

Echelmeyer K, Wang Z. 1987. Direct observation of basal sliding and deformation of basal drift at sub-freezing temperatures. *Journal of Glaciology* **33**(113): 83–98.

Endres AL, Murray T, Booth AD, West JL. 2009. A new framework for estimating englacial water content and pore geometry using combined radar and seismic wave velocities. *Geophysical Research Letters* **36**: L04501.

Folk RL, Ward WC. 1957. Brazos River bar: a study in the significance of grain size parameters. *Journal of Sedimentary Petrology* **27**: 3–26.

Fountain AG, Walder JS. 1998. Water flow through temperate glaciers. *Reviews of Geophysics* **36**(3): 299–328.

Fountain AG, Schlicting RB, Jacobel RW, Jansson P. 2005. Fractures as main pathways of water flow in temperate glaciers. *Nature* **433**: 618–621.

Gades AM, Raymond CF, Conway H, Jacobel RW. 2000. Bed properties of Siple Dome and adjacent ice streams, West Antarctica, inferred from radio-echo sounding measurements. *Journal of Glaciology* **46**(152): 88–94.

Gulley JD, Benn DI, Screaton E, Martin J. 2009. Mechanisms of englacial conduit formation and their implications for subglacial recharge. *Quaternary Science Reviews* **28**: 1984–1999.

Hart JK, Martinez K. 2006. Environmental sensor networks: a revolution in the earth system science? *Earth Science Reviews* **78**: 177–191.

Hart JK, Waller RI. 1999. An investigation of the debris-rich basal ice from Worthington Glacier, Alaska. *USA Journal of Glaciology* **45**: 54–56.

Hart JK, Martinez K, Ong R, Riddoch A, Rose KC, Padhy P. 2006. An autonomous multi-sensor subglacial probe: design and preliminary results from Briksdalsbreen, Norway. *Journal of Glaciology* **52**(178): 389–397.

Hart JK, Rose KC, Martinez K, Ong R. 2009. Subglacial clast behaviour and its implication for till fabric development: new results derived from wireless subglacial probe experiments. *Quaternary Science Reviews* **28**: 597–607.

Hart JK, Rose KC, Martinez K. 2011a. Temporal englacial and subglacial water variability associated with a rapidly retreating glacier. *Earth Surface Processes and Landforms* **36**: 1230–1239.

Hart JK, Rose KC, Waller RI, Vaughan-Hirsch D, Martinez K. 2011b. Assessing the catastrophic break up of Briksdalsbreen, Norway, associated with rapid climate change. *Journal of Geological Society of London* **168**: 1–16.

Hausmann H, Behm M. 2011. Imaging the structure of cave ice by ground-penetrating radar. *The Cryosphere* **5**: 329–340.

Hock R, Hooke RL. 1993. Evolution of the internal drainage system in the lower part of the ablation area of Storglaciären, Sweden. *Geological Society of America Bulletin* **105**: 537–546.

Hooke RLeB, Dahlin BB, Kauper MT. 1972. Creep of ice containing dispersed fine sand. *Journal of Glaciology* **11**(63): 327–336.

Hooke RLeB, Laumann T, Kohler J. 1990. Subglacial water pressures and the shape of subglacial conduits. *Journal of Glacialogy* **36**: 67–71.

Iken A, Echelmeyer K, Harrison W, Funk M. 1993. Mechanisms of fast flow in Jakobshavn Isbræ, West Greenland: Part I. Measurements of temperature and water level in deep boreholes. *Journal of Glaciology* **39**(131): 15–25.

Iken A, Bindschadler RA. 1986. Combined measurements of subglacial water pressure and surface velocity Findelengletscher, Switzerland: conclusions about drainage system and sliding mechanism. *Journal of Glaciology* **32**: 101–119.

Irvine-Fynn TDL, Moorman BJ, Williams JLM, Walter FSA. 2006. Seasonal changes in ground-penetrating radar signature observed at a polythermal glacier, Bylot Island, Canada. *Earth Surface Processes and Landforms* **31**: 892–909.

Jacobel R, Raymond C. 1984. Radio echo-sounding studies of englacial water movement in Variegated Glacier, Alaska. *Journal of Glaciology* **30**: 22–29.

Jacobel RW, Welch BC, Osterhouse D, Pettersson R, MacGregor JA. 2009. Spatial variation of radar-derived basal conditions on Kamb Ice stream. *Annals of Glaciology* **50**(51): 10–16.

Jacobel RW, Lapo KE, Stamp JR, Youngblood BW, Welch BC, Bamber JL. 2010. Comparison of basal reflectivity and ice velocity in east Antarctica. *The Cryosphere* **4**: 447–452.

Jansson P, Hock R, Schneider T. 2003. The concept of glacier storage – a review. *Journal of Hydrology* **282**: 116–129.

Jóhannesson H, Sæmundsson K. 1998. Geological Map of Iceland, 1:500 000: Bedrock Geology, Icelandic Institute of Natural History.

Kamb B. 1991. Rheological nonlinearity and flow instability in the deforming bed mechanism of ice stream motion. *Journal of Geophysical Research* **96**: 16585–16595.

Kulessa B, Booth AD, Hobbs A., Hubbard AL. 2008. Automated monitoring of subglacial hydrological processes with ground-penetrating radar (GPR) at high temporal resolution: scope and potential pitfalls. *Geophysical Research Letters* **35**: L24502. DOI: 10.1029/2008GL035855.

Lawson W, Elliott C. 2003. Strain-rate effects on the strength of debris-laden glacier ice. *New Zealand Journal of Geology and Geophysics* **46**: 323–330.

Lichtenecker K. 1926. Die dielektrizitatskonstante naturlicher und kunstlicher mischkorper. *Physikalische Zeitschrift* **27**: 115–158.

Looyenga H. 1965. Dielectric constant of heterogeneous mixtures. *Physica* **31**(3): 401–406.

MacGregor JA, Winebrenner DP, Conway H, Matsuoka K, Mayewski PA, Clow GD. 2007. Modeling englacial radar attenuation at Siple Dome, West Antarctica, using ice chemistry and temperature data. *Journal of Geophysical Research* **112**: F03008. DOI: 10.1029/2006JF000717.

Macheret YY, Glazovsky AF. 2000. Estimation of absolute water content in Spitsbergen glaciers from radar sounding data. *Polar Research* **19**: 205–216.

Macheret YY, Moskalevsky MY, Vasilenko EV. 1993. Velocity of radio waves in glaciers as an indicator of their hydrothermal state, structure and regime. *Journal of Glaciology* **39**: 373–384.

Mair D, Nienow P, Sharp MJ, Wohlleben T, Willis I. 2002. Influence of subglacial drainage system evolution on glacier surface motion: Haut Glacier d'Arolla, Switzerland. *Journal of Geophysical Research* **107**(B8): 2175.

Mair A, Willis I, Fischer UH, Hubbard B, Nienow P, Hubbard A. 2003. Hydrological controls on patterns of surface, internal and basal motion during three 'spring events'': Haut Glacier d'Arolla, Switzerland. *Journal of Glaciology* **49**(167): 555–567.

Martinez A, Byrnes AP. 2001. Modeling dielectric-constant values of geologic materials: an aid to ground-penetrating radar data collection and interpretation. *Current Research in Earth Sciences, Bulletin 247, Part 1*. (*http://www.kgs.ukans.edu/Current/2001/martinez/martinez1.hmtl*)

Martinez K, Hart JK. 2010. Glaciers monitoring: deploying custom hardware in harsh environments. In Wireless Sensor Networks - Deployments and Design Framework, Gaura E, Allen M, Girod L, Challen G (eds). Springer: US; 245–258.

Martinez K, Hart JK, Ong R. 2009. Deploying a wireless sensor network in Iceland. *Lecture Notes in Computer Science, Proceedings of the Geosensor Networks* **5659**: 131–137.

Matsuoka K, Morse D, Raymond CF. 2010. Estimating englacial radar attenuation using depth profiles of the returned power, Central West Antarctica. *Journal of Geophysical Research* **115**: F02012. DOI: 10.1029/2009JF001496, 2010.

Moorman BJ, Michel FA. 1998. The Application of Ground-Penetrating Radar to the Study of Glacial Hydrology. GPR '98: Seventh International Conference on Ground-Penetrating Radar, The University of Kansas, Lawrence, Kanasas, USA, May 27–30, 1998.

Murray T, Stuart GW, Fry M, Gamble NH, Crabtree MD. 2000. Englacial water distribution in a temperate glacier from surface and bore hole radar velocity analysis. *Journal of Glaciology* **46**(154): 389–398.

Murray T, Booth A, Rippin D. 2007. Limitations of glacier ice-water content estimated using velocity analysis of surface ground-penetrating radar surveys. *Journal of Environmental and Engineering Geophysics* **12**: 87–99.

Nienow P, Sharp M, Willis I. 1998. Seasonal changes in the morphology of the subglacial drainage system, Haut Glacier d'Arolla, Switzerland. *Earth Surface Processes and Landforms* **23**: 825–843.

Nye JF. 1952. The mechanics of glacier flow. *Journal of Glaciology* **2** (11): 52–53.

Nye JF. 1973. Water at the bed of an ice sheet. *IAHS* **95**: 189–194.

Olhoeft GR. 1989. Electrical properties of rocks. In Physical Properties of Rocks and Minerals, Touloukian YS, Judd WR, Roy RF (eds). Hemisphere Publishing Corporation: New York; 257–329.

Paterson WSB. 1994. The Physics of Glaciers, 3rd edn. Oxford Press/Butterworth-Heinemann: Oxford.

Pettersson R, Jansson P, Holmlund P. 2003. Cold surface layer thinning on Storglaciaren, Sweden, observed by repeated ground penetrating radar surveys. *Journal of Geophysical Research* **108**(F1): 6004, doi:10.1029/2003JF000024.

Pohjola VA 1993. TV-video observations of bed and basal sliding on Storglaciären, Sweden. *Journal of Glaciology*, **39**(131): 111–118.

Raymond CF, Harrison WD. 1975. Some observations on the behavior of liquid and gas phases in temperate glacier ice. *Journal of Glaciology* **14**: 213–233.

Rippin D, Willis I, Arnold N, Hodson A, Moore J, Kohler J, Björnsson H. 2003. Changes in geometry and subglacial drainage of Midre Lovénbreen, Svalbard determined from digital elevation models. *Earth Surface Processes and Landforms* **28**: 273–298.

Rose KC, Hart JK, Martinez K. 2009. Seasonal changes in basal conditions at Briksdalsbreen, Norway: the winter–spring transition. *Boreas* **38**: 579–590.

Röthlisberger H. 1972. Water pressure in intra- and sub-glacial channels. *Journal of Glaciology* **11**: 177–203.

Shreve RL. 1972. Movement of water in glaciers. *Journal of Glaciology* **11**: 205–214.

Sigurðsson O. 1998. Glacier variations in Iceland 1930–1995. *Jökull* **45**: 3–25.

Sihvola A, Nyfors E, Tiuri M. 1985. Mixing formulae and experimental results for the dielectric constant of snow. *Journal of Glaciology* **31**: 163–170.

Sugiyama S, Skvarca P, Naito N, Enomoto H, Tsutaki S, Tone K, Marinsek S, Aniya M. 2011. Ice speed of a calving glacier modulated by small fluctuations in basal water pressure. *Nature Geoscience* **4**: 597–600. DOI: 10.1038/ngeo1218.

Walder JS, Fowler A. 1994. Channelized subglacial drainage over a deforming bed. *Journal of Glaciology* **40**: 3–15.

West JL, Rippin DM, Murray T, Mader HM, Hubbard B. 2007. Dielectric permittivity measurements on ice cores: implications for interpretation of radar to yield glacial unfrozen water content. *Journal of the Environment English Geophysics* **12**(1): 37–45.

Wharton RP, Hazen GA, Rau RN, Best DL. 1980. Electromagnetic propagation logging: advances in technique and interpretation. In 55th Annual Fall Technical Conference and Exhibition, 21–24 September, Dallas, Texas. Dallas, TX, Society of Petroleum Engineers. (SPE Paper 9267.)

Willis IC, Sharp MJ, Richards KS. 1990. Configuration of the drainage system of Midtdalsbreen, Norway, as indicated by dye-tracing experiments. *Journal of Glaciology* **36**(122): 89–101.

Willis IC, Fitzsimmons C, Melvold K, Andreassen LM, Giesen RH. 2012. Structure, morphology and water flux of a subglacial drainage system, Midtdalsbreen, Norway. *Hydrological Processes*. DOI: 10.1002/hyp.8431.

Winebrenner DP, Smith BE, Catania GA, Conway HB, Raymond CF. 2003. Radio-frequency attenuation beneath Siple Dome, West Antarctica, from wide-angle and profiling radar observations. *Annals of Glaciology* **37**: 226–232.

Zakri T, Laurent J-P, Vauclin M. 1998. Theoretical evidence for 'Lichtenecker's mixture formulae' based on effective medium theory. *Journal of Physics D: Applied Physics* **31**: 1589–1594.

Zwally HJ, Abdalati W, Herring T, Larson K, Saba J, Steffen K. 2002. Surface melt-induced acceleration of Greenland ice-sheet flow. *Science* **297**: 218–222.